Efficient Propulsion for the Tethys Long-Range Autonomous Underwater Vehicle

James G. Bellingham[1*], Yanwu Zhang[1], Justin E. Kerwin[2], Jonathan Erikson[1], Brett Hobson[1], Brian Kieft[1], Michael Godin[1], Robert McEwen[1], Thomas Hoover[1], James Paul[3], Andrew Hamilton[1], Jeffrey Franklin[3], and Andrew Banka[3]
* Corresponding author: jgb@mbari.org

***Abstract* — The Tethys autonomous underwater vehicle (AUV) is a 110 kg vehicle designed for long-range, high-endurance operations. Performance goals include supporting a payload power draw of 8 W for a range of 1000 km at 1 m/s, and a power draw of 1 W for 4000 km at 0.5 m/s. Achieving this performance requires minimizing drag and maximizing propulsion efficiency. In this paper, we present the design of the propulsion system, explore the issues of propeller-hull interactions, and present preliminary test results of power consumption and efficiency. In recent underwater experiments, the propulsion system's power consumptions were measured in both Bollard pull tests and during the vehicle's flights. Preliminary results of power consumptions and efficiency are shown to be close to the theoretical predictions.**

I. Introduction

The Tethys AUV (Figure 1) operational characteristics are designed to fall between those of existing gliders and propeller-driven AUVs. Gliders in operation today are capable of ranges of thousands of kilometers, but these ranges are only achieved at low speeds and with low payload power consumption, e.g. 0.3 m/s and 1 W [1]. Propeller-driven AUVs such as Dorado can carry comprehensive payloads at higher speeds but at the cost of a shorter range [2]. For example, MBARI's 6000 m rated Dorado mapping vehicle carries multibeam, sidescan, and sub-bottom profiling sonars consuming more than 200W at 1.5 m/s for ranges on the order of 100 km. The Tethys AUV (2.3 m long with a mid-section diameter of 12 inches) is designed to carry larger payloads and operate faster than today's gliders, while achieving a much greater range than today's propeller-driven AUVs.

Initial development of Tethys has been motivated by the desire for biological observations and process experiments. A summary of needs includes the abilities to:

- Continuously observe a phytoplankton bloom from 'boom to bust' – perhaps 4 weeks.
- Carry sensors and samplers to characterize marine microbial ecosystems.
- Transit thousands of kilometers to regions of interest.
- Operate in teams of multiple vehicles to quantify budgets and rates of fast-changing chemical and biological parameters.
- Observe interactions between trophic levels of marine ecosystems (this may also require multi-vehicle operations).
- Be affordable by individual investigator laboratories.
- Be simple to operate.
- Ultimately be operable independent of ships through the global ocean.

For example, observations of chemical and biological variability off the west coast of the United States motivate an ability to survey at least 500 km from shore. This operational range allows a vehicle to operate both within the nutrient rich upwelling system present in the nearshore region, and in the nutrient poor California Current system offshore. A range of 4000 km enables the vehicle to transit from the continental U.S. west coast all the way to Hawaii.

We met these needs by creating a vehicle capable of running in multiple operational modes. The vehicle can transit while preserving onboard energy by running at low speed mode with most sensors powered off. A variable buoyancy system allows the vehicle to be ballasted to drift at depth while consuming almost no power. The vehicle can run at a higher speed with all sensors powered to conduct survey operations. By combining these capabilities, a diverse range of payloads and missions can be supported.

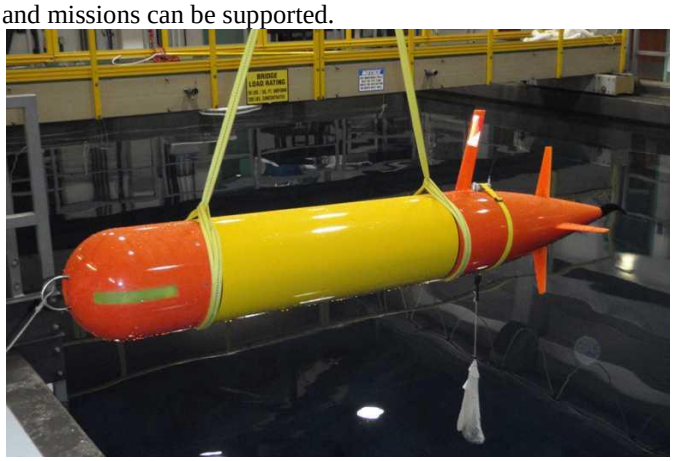

Figure 1: The Tethys AUV suspended over MBARI's test tank. The left orange section of the vehicle is the payload volume. The yellow center section is the main pressure vessel housing vehicle electronics and batteries. To the right is the propulsion and control section, which also includes an antenna (orange mast) for Iridium, GPS, and line-of-sight wireless comms.

[1] Monterey Bay Aquarium Research Institute, 7700 Sandholdt Road, Moss Landing, CA 95039
[2] Professor Emeritus of Massachusetts Institute of Technology
[3] Airflow Sciences Corporation, 12190 Hubbard Street, Livonia, MI 48150

Proc. IEEE AUV'2010, pp. 1-6,
Monterey, CA, September 2010.

An example mission might involve the following: a) conduct a slow, power conserving run 500 km offshore, b) wait in drift mode until an event occurs, surfacing once per day for satellite communications with shore, c) on detection of the event, use the high speed mode to map out local variability, d) finally, return to shore at low speed. Conversely a simpler mission might be to simply run offshore 500 km and back at high speed to obtain a section of water column properties. Yet a third mission might involve operating a high-power payload intermittently, alternating long, low-speed runs with short, high-power observational activities.

From these general needs and operational concepts we distilled a set of design requirements, which were: a vehicle weight on the order of 100 kg, a range of 1000 km at 0.75 m/s with a 8 W hotel load, a range of 3000 km at 0.35 m/s and minimal payload draw, and the ability to ballast to neutral buoyancy and drift at depth. During the design process described below, it became clear that greater performance was possible, and the high and low speeds where adjusted upwards to 1.0 and 0.5 m/s, respectively, and the lower range target was increased to 4000 km.

A. Vehicle Sizing: Range, Speed, and Hotel Load

The range of an underwater vehicle depends on vehicle size, speed, and hotel load, where hotel load is defined as power consumption by non-propulsion systems. Identification of a representative initial payload is critical for the vehicle design process, as this allows estimation of hotel loads. For our first payload we selected sensors for temperature, salinity, dissolved oxygen, optical backscatter, fluorescence, nitrate, and water velocity. Operated at a reasonable duty cycle, we estimate a hotel load of 8W is achievable.

To determine the maximum range, we start by describing the total power draw as a function of speed:

$$P = P_{prop} + H \quad \text{where} \quad P_{prop} = \frac{1}{2}\frac{C_D A \rho v^3}{\eta} \tag{1}$$

The total power draw P is thus the sum of propulsion power P_{prop} and hotel load H. Hotel load is simply the power consumed by all subsystems other than propulsion. Propulsion power is a function of the drag coefficient of the vehicle, C_D, the area of the vehicle, A, the density of water, ρ, the speed of the vehicle, v, and the efficiency of the propulsion system, η. For the calculations below, we assume propulsion efficiency and vehicle drag are independent of speed.

By minimizing power consumption per unit distance traveled as a function of speed, one can arrive at the optimum vehicle speed and the maximum range:

$$v_{opt} = \left(\frac{\eta H}{C_D A \rho}\right)^{1/3} \tag{2}$$

and

$$d_{\max} = \frac{2E_{cap}}{3}\left(\frac{\eta}{C_D A \rho H^2}\right)^{1/3} \tag{3}$$

Here E_{cap} is the energy stored in onboard batteries.

Using these relationships, we can plot the optimum speed and maximum range for a given set of vehicle characteristics to understand performance characteristics. In Figure 2, the curves are plotted for a C_D A product of 0.014 square meters, η = 0.5, and E_{cap} = 38 MJ, which correspond to the initial estimates for a 110 kg Tethys.

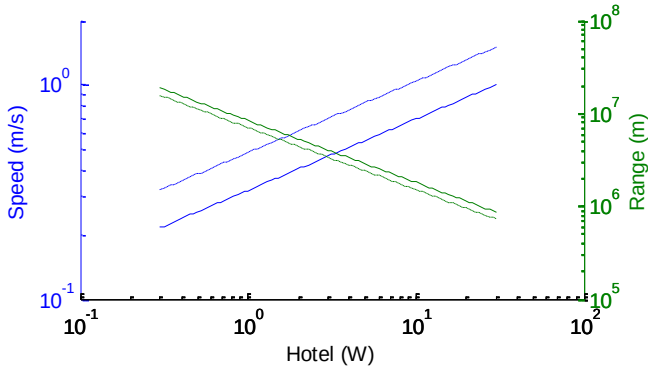

Figure 2: Optimum speed and maximum range are plotted as solid blue and green lines for the candidate vehicle described in text. The dashed lines show the comparative insensitivity to small increments in speed, showing a speed 150% the optimum speed, and the resulting range.

B. Propeller versus Buoyancy Driven Propulsion

Given the desire for extended endurance, and the superior performance range characteristics of existing gliders, an obvious question is: why use a propeller for propulsion? Why not build a more powerful glider or a hybrid system with both propeller and buoyancy-driven propulsion? The decision to focus on a propeller-driven system for propulsion was primarily driven by the determination that such a propulsion system could provide efficient propulsion across the range of speeds desired, and thus a adding a second mode of propulsion was unnecessary. Using buoyancy-driven propulsion as the sole propulsion system was discounted both for reasons of flexibility and sizing. The first issue revolves around the need for buoyancy-driven systems to fly yo-yo type vertical profiles, in contrast to nearly unconstrained vertical flight profile of propeller-driven systems. The sizing issue revolves around the quadratic growth of propulsion force with speed. In a buoyancy-driven system, propulsion force is created by volume change, and thus four times the volume change is required to double the speed. In effect a larger and larger fraction of the vehicle must be used for the propulsion system, which in turn reduces battery and/or payload capacity and drives the vehicle size up.

II. Approach: Minimizing Propulsion Power Consumption

Optimization of vehicle performance is closely tied to minimizing power consumed by propulsion. For the Tethys vehicle, this process started with the design of a low drag hull. Using computation fluid dynamics (CFD) modeling, the wake of the hull was determined, which in turn allowed the design of a propeller that optimally interacts with the wake. The propeller design was followed by selection of a high

performance electric motor and drive train to complete the system. Details of the process are described below.

A. Minimizing Drag

By employing potential flow analysis followed by 3-D viscous CFD modeling, we designed a low-drag hull. A constraint on the hull design was the desire to have an extendable vehicle to accommodate a range of payloads, thus a parallel midbody design was selected. Assuming a simple drag model of a vehicle (using only frontal and surface drag coefficients) with a hemispherical nose, parallel body, conical tail, and 110-kg displacement, a minimum drag coefficient was found at a mid-section diameter of 12 inches (0.3 m). This dimension was used to constrain the potential flow and CFD analyses that followed.

The drag on the Tethys body is composed of skin friction, which is related to the surface area of the AUV, and form-drag, which is a function of the AUV shape. Drag minimization focused on reducing the form drag. For minimum drag, the flow that accelerates around the forward portion of the body must follow the contour of the tail as it decelerates and fills in the wake region of the AUV. If the flow is decelerated too quickly or the body curves too sharply, the flow will "separate" from the AUV rather than following its shape. In that case, the remainder of the AUV tail would feel the reduced pressure. The result would be additional drag.

The ability of the flow to "turn" and follow the contour of the body is related to the kinetic energy in the flow near the body surface. Since the kinetic energy will decrease as the flow decelerates, the tail shape was chosen such that the curvature varied from a finite value at the body/tail junction to zero at the tip of the tail. The body diameter and tail length were then used to define the coefficients for the resulting body shape function. Potential flow analyses along with the Stratford boundary layer separation criteria verified that the flow would remain attached along the length of the body at both the 1 m/s and 0.5 m/s speeds.

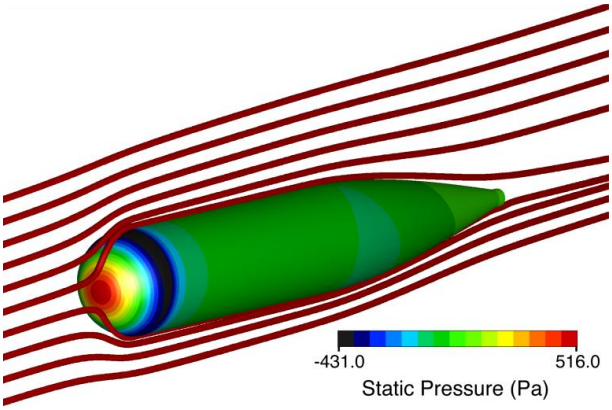

Figure 3. Flow streamlines and surface pressure distribution at 1 m/s and 3º pitch. The effect of the pitch angle can be seen in the flow streamlines and angled pressure distribution. Pressure rises toward the tail, indicating pressure recovery that helps reduce drag.

Next, CFD analyses were used to evaluate the flow field around the Tethys AUV for both forward speeds and for pitch angles of 0 and 3 degrees. Pitch is used to alter the vertical location of the AUV, so it is important to ensure that the drag remains low at these moderate angles. The commercial CFD program Fluent was used to simulate these flow fields and determine the drag, lift, and pitching moment coefficients for use in dynamic performance evaluations. Results from the 1 m/s, 3º pitch case are shown in Figure 3. The CFD results also provided input to the propeller design process (described below). Later simulations included the effect of the propeller thrust on the overall flow field and AUV drag, as shown in Figure 4.

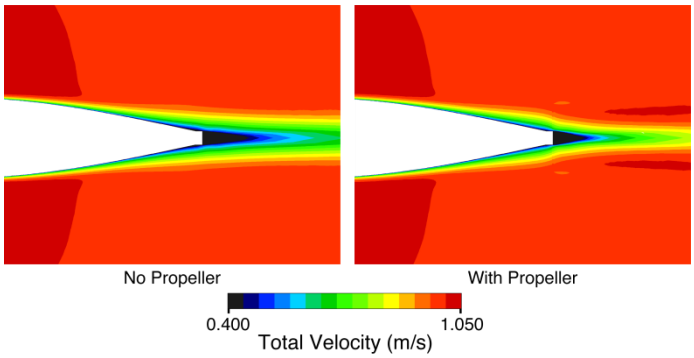

Figure 4. Propeller thrust alters the flow near the tail, narrowing the wake profile.

B. Propeller Design and Manufacture

We designed a single propeller for two vehicle speeds: 1 m/s and 0.5 m/s. The 2-blade propeller has a diameter of 10 inches (0.25 m) and spins at 300 revolutions per minute (RPM) and 150 RPM for the 1 m/s and 0.5 m/s vehicle speeds, respectively. Vehicle performance goals required propeller efficiency of no less than 0.8 for both speeds, which posed a challenge in the design. The propeller's thrust is required to counteract the expected drag force (including that of the control surfaces and the increased drag due to surface roughness) at the two vehicle speeds.

It is important to obtain the wake profile upstream of the propeller in order to optimize the propeller design. The wake profile in the absence of the propeller (i.e., the nominal wake) was calculated by Airflow Sciences Corporation using 3-D CFD software and appropriate boundary layer representations. However, with the propeller present, the flow through the propeller plane is contracted and accelerated, thereby modifying the wake profile. The MIT Propulsor Lifting Line (PLL) program [3] took in the nominal wake profile and calculated the modified wake profile (called the effective wake profile) as well as the propeller-induced velocity, the sum of which gave the total velocity field. Note that the wake profiles for the two vehicle speeds are different, adding yet another challenge to the propeller design. By running the PLL program, we generated a preliminary blade design that met the thrust and efficiency requirements.

After the completion of the parametric study using the PLL theory, the next step was the final blade design for

manufacture. This was carried out using a coupled Euler/lifting-surface code initially developed at MIT [4-5]. This procedure extended the lifting-line results in the following ways:

- Accounts for the actual tapered shape of the Tethys AUV afterbody in the hydrodynamic solution.
- Directly computes the convection of the body boundary layer vorticity resulting from the propeller-induced flow rather than approximating it.
- Represents the propeller blades by lifting surfaces rather than lifting lines.
- Analyzes the design geometry in different operating conditions, specifically for the 1.0 m/s and 0.5 m/s operating points.
- Introduces the effect of the Reynolds number (which is different for the two operating conditions) on blade section viscous drag and reduction of lift into the calculation based on results at a series of radii obtained from a two-dimensional airfoil boundary layer code [6].
- Directly uses the same detailed blade surface geometry for manufacture as that used in the hydrodynamic calculations can be used directly for manufacture.

Figure 5 shows how the body boundary layer is introduced into the calculation. The curve labeled "Target wake" is the boundary layer profile at the location of the propeller (but with no propeller present) as calculated by Airflow Sciences Corporation's CFD code. The curve labeled "new inflow" is the computed inflow profile several propeller radii upstream that results in a velocity at the propeller matching the specified profile. This is done by introducing inlet losses iteratively in the Euler solver until a match is achieved. These inlet losses are then used in the coupled calculations with the propeller present. The same procedure was used for the 0.5 m/s operating condition.

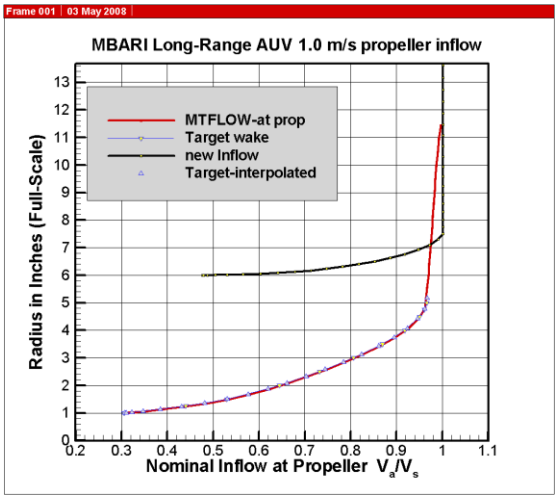

Figure 5. Propeller inflow profile and wake profile.

Figure 6 shows the computed sectional drag coefficient as a function of blade span for the two operating conditions. It shows that the drag coefficient is high at the inner radii where the local sectional Reynolds numbers are extremely low. For best efficiency, it is therefore essential to keep the blade area and the number of blades as low as possible. It is also necessary to keep the thickness of the blade sections to an absolute minimum. Large ship propellers are stress limited at the innermost radii and need thick sections. But at the size and power of the Tethys AUV, this is not a factor so that the sections could be made much thinner. In addition, at this low Reynolds number the optimum section shape turns out to have a relatively thick trailing edge [6].

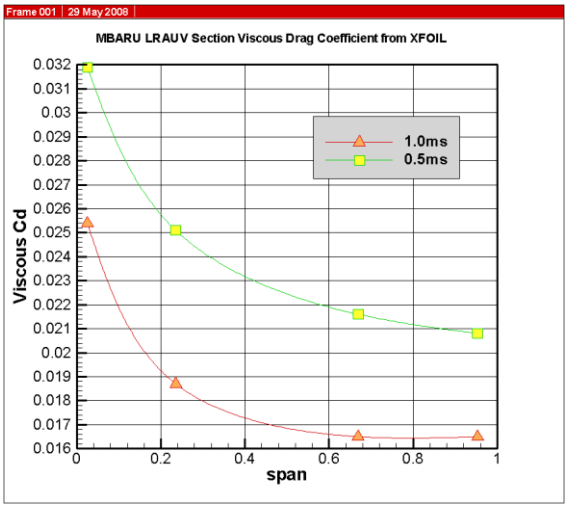

Figure 6. Propeller's sectional viscous drag coefficient for the two vehicle speeds.

Figure 7 shows the geometry of a single blade. We used SolidWorks to generate a solid shape, and then generated a stereolithography file that was read by a Fused Deposition Modeling machine (FDM) to create a solid plastic part that became the pattern for a silicone mold. A glass fiber filled urethane was then used to cast a working part from the mold.

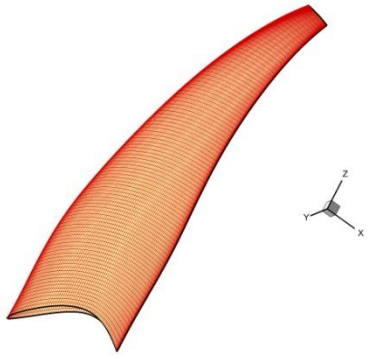

Figure 7. Geometry of the propeller blade.

C. Motor Selection

The drive motor, drive train, and propeller on Tethys must operate near maximum efficiency in both the low and high speed modes. To achieve this over a doubling of rotational speed and quadrupling of torque is a challenge. For example, the low speed operation of Tethys at 0.5 m/s requires 2 N of thrust, which can be generated with only 0.07 Nm of torque from the motor. At these low speeds and torques, the system is particularly sensitive to parasitic friction and losses.

Most AUV drive motors, including MBARI's Dorado's, use a motor with a gear reduction to allow the motor to run at the higher speeds where the motor is more efficient, and turn the propeller at lower speeds where the propeller is more efficient. The motor and gear box are usually flooded in pressure compensating oil so there are no large pressure differentials across the dynamic shaft seal. The problem with using this design for Tethys was the free-running frictional torque of a gear motor running in oil with a seal could easily exceed the torque required to propel the vehicle, resulting in very low propulsion efficiencies.

On Tethys, an open-frame, 16 pole permanent magnet motor is mounted between two precision ball bearings within the one atmosphere pressure case. The rotor directly turns the propeller drive shaft through magnetic coupling. The pressure boundary inside the magnetic coupling for the 300-m depth operation was fabricated from non-conductive PEEK plastic to reduce any eddy-current losses. A hollow fiberglass drive shaft with bonded titanium bearing supports three water-lubricated glass ball/delrin plastic race ball bearings. The motor is electrically driven with a full wave, trapezoidal drive.

III. Test Results

A. Hull Drag Verification

To validate the drag calculated by CFD, we created a half scale model of the hull shape and measured the drag in the MBARI test tank (15 m long, 10 m wide, 10 m deep, filled with seawater). In consideration of the relatively short length of the tank, we designed a tow rig consisting of pulleys and Kevlar strings to tow the model at different speeds. Using this rig, we could keep the model traveling in a straight line, accelerate it to the desired speed, sustain the desired speed and finally stop it before it collided with the opposite side of the tank.

The tow speed was measured by way of a spindle that was placed on the shaft of an optical encoder. The force was measured by a load cell. To account for frictional losses in the pulleys and string guides as well as drag losses of the string in the water, a "string only" test was run. The steady-state frictional loss term was then subtracted from the drag measured during the model test. The resulting data points are then plotted as drag as a function of speed and compared with the drag calculated by CFD, as shown in Figure 8. Note that the drag measurements on the half model have been converted to that of the full-size model. The measured drag appeared to be lower than the drag calculated by CFD. Note that the half-model test only provides an approximation for the full-size hull. While the discrepancy demands further analysis, this comparison gave us confidence to proceed with full size construction of the Tethys vehicle.

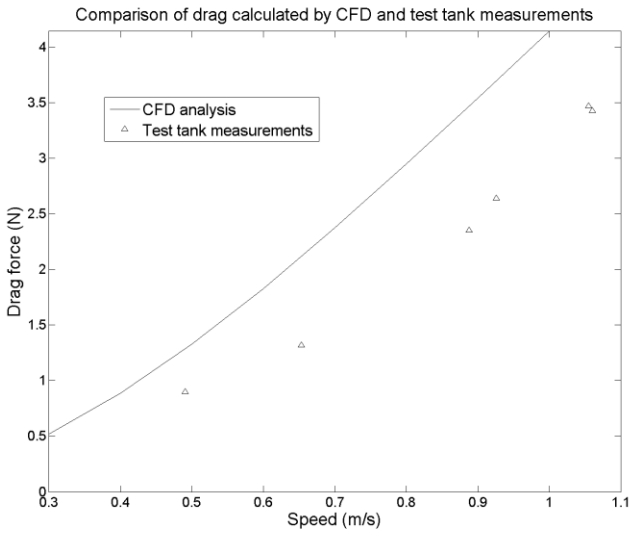

Figure 8. Comparison of the CFD-calculated drag and the measured drag.

B. Static Thrust Test (i.e., Bollard Pull Test)

After mounting the 2-blade propeller on the full-size vehicle, we conducted bollard pull tests in the MBARI test tank to verify the static thrust provided by the propeller. As shown in Table I, the measured bollard pull force was within 14% of that predicted by the MIT propeller design code at both operating points (150 RPM and 300 RPM).

Table I. Bollard pull force comparison

	Predicted by MIT propeller design code	Measured
150 RPM	4.0 N	4.4 N
300 RPM	16.0 N	18.2 N

C. Preliminary Power Consumption Test

We did a preliminary power consumption test on the Tethys AUV in a level flight. The desired vehicle speed was 1 m/s (propeller spinning at 300 RPM), but the actual vehicle speed was 0.96 m/s (measured by an onboard LinkQuest Doppler Velocity Log (DVL)), because the vehicle was flying at a small negative pitch angle to counteract positive buoyancy, which increased the drag and decreased the vehicle speed.

At this speed, the measured power consumed by the vehicle's propulsion system (composed of the motor system and the propeller) was about 12 W. Thus the measured propulsion system's efficiency was

$$\eta_{meas} = \frac{thrust[speed(1-w)]}{Pwr_{in}} = \frac{7 \times [0.96 \times 0.87]}{12} = 0.49$$

where the 7 N thrust (drag) has accounted for the additional drag due to the vehicle's control surfaces, instrument ports, and surface roughness; w is the Taylor wake fraction.

In comparison, the expected efficiency of the propulsion system is

$$\eta_{expected} = \eta_{motor\_system} \times \eta_{propeller} = 0.66 \times 0.8 = 0.53$$

where $\eta_{motor\_system} = 0.66$ was based on power consumption measurements of the motor system (including the motor and the motor controller) using a dynamometer. The discrepancy between the expected and measured efficiencies is about 8% of either. We found that the current motor system's efficiency is reduced by an inefficient motor controller, which brings down the propulsion system's overall efficiency. We intend to replace the motor controller with one that is more efficient and consumes less power.

IV. Conclussions

A small, high-performance AUV has been developed with superior range characteristics as compared with existing propeller-driven AUVs. The vehicle is capable of operating efficiently at speeds of 0.5 and 1.0 m/s. Tests of the propulsion system and of the operational vehicle validates a range of 1000 km or greater at the higher speed. Low speed performance is in the process of being characterized. Modeling indicates that efficient performance should extend to speeds well above the initial design targets.

Acknowledgment

This work was supported by the David and Lucile Packard Foundation and the Office of Naval Research (ONR) under grant N00014-02-1-0856. The authors are thankful to James Scholfield and the MBARI machine shop for mechanical work, to Edward Mellinger, Chad Kecy, and Jose Rosal for work on the motor system and electronics, to MBARI interns Francois Cazenave and Brian Hoover for their help with the drag measurements in the test tank, and to MBARI intern Brooks Reed for helping with the buoyancy engine design.

References

[1] D. L. Rudnick, R. E. Davis, C. C. Eriksen, D. M Fratantoni, and M. J. Perry, "Underwater Gliders for Ocean Research," *Marine Technology Society Journal*, Vol. 38, No. 2, pp. 73-84, 2004.

[2] M. Sibenac, W. J. Kirkwood, R. McEwen, F. Shane, R. Henthorn, D. Gashler, and H. Thomas, "Modular AUV for Routine Deep Water Science Operations," Proc. MTS/IEEE Oceans'02, pp. 167-172, Biloxi, MS, October 2002.

[3] W. B. Coney, MIT-PLL Propulsor Lifting Line Code User's Manual, Massachusetts Institute of Technology Department of Ocean Engineering, November 1988.

[4] J. E. Kerwin, D. P. Keenan, S. D. Black, and J. G. Diggs, "A Coupled Viscous/Potential Flow Design Method for Wake-Adapted, Multi-Stage, Ducted Propulsors," Proc. Society of Naval Architects and Marine Engineers, 1994.

[5] J. E. Kerwin, T. J. Michael, and S. K. Neely,"Improved Algorithms for the Design/Analysis of Multi-Component Complex Propulsors," Proc. 11th Propellers/Shafting Symposium, Society of Naval Architects and Marine Engineers, Williamsburg, VA, September 2006.

[6] M. Drela, "XFOIL: An Analysis and Design System for Low Reynolds Number Aerofoils," Lecture Notes in Engineering (Volume 54, Low Reynolds Number Aerodynamics), New York, NY: Springer-Verlag, 1989.

[7] M. Drela, "Integral Boundary Layer Formulation for Blunt Trailing Edges," AIAA, 89-2200, 1989.